Letter

Electromagnetic origin of the microwave absorption response of Fe_3O_4 thin films

James Wampler,[1,*] Nelson Hua,[1] Roopali Kukreja,[1,2,3] Juan Gabriel Ramírez,[4] Ali C. Basaran,[1] Eric E. Fullerton,[2] Oleg Shpyrko,[1] and Ivan K. Schuller[1]

[1]*Department of Physics and Center for Advanced Nanoscience, University of California San Diego, La Jolla, California 92093, USA*
[2]*Center for Memory and Recording Research, University of California San Diego, La Jolla, California 92093-0401, USA*
[3]*Department of Materials Science Engineering, University of California Davis, Davis, California 95616, USA*
[4]*Department of Physics, Universidad de los Andes, Bogotá 111711, Colombia*

(Received 6 October 2021; revised 9 June 2022; accepted 6 July 2022; published 10 August 2022)

Low-field microwave absorption techniques are ultrasensitive, nondestructive methods for probing electric and magnetic properties of solids. Nonresonant low-field microwave absorption techniques such as magnetic field modulated microwave spectroscopy (MFMMS) can easily detect electromagnetic phase transitions in minute and inhomogeneous samples. While this technique can easily and almost selectively identify superconducting transitions, magnetic phase transitions produce more varied responses. Here, we present a technique to investigate the electric and magnetic properties of a sample with complex electromagnetic responses. This technique involves taking a series of magnetic hysteresis loops and magnetoresistance measurements. These can be compared to MFMMS data to identify features having electric or magnetic origin. This approach is applied to magnetite (Fe_3O_4), which possesses an electric, magnetic, and structural phase transition across its Verwey transition. By measuring high-quality Fe_3O_4 thin films in MFMMS and complementary techniques, the previously inscrutable MFMMS signal is analyzed. Furthermore, a model of the MFMMS signal can be calculated from the magnetic and electric data, which reproduces most of the features of the experimentally obtained MFMMS signal. This technique broadens the capabilities of MFMMS beyond the detection of superconductors.

DOI: 10.1103/PhysRevB.106.L060402

I. INTRODUCTION

Magnetic field modulated microwave spectroscopy (MFMMS) is a fast, ultrasensitive technique, adapted from older low-field microwave absorption techniques [1,2]. MFMMS is based on a modified electron paramagnetic resonance (EPR) technique. It measures the change in the absorbed microwave power in a microwave cavity. In a typical measurement, a fixed DC field and a smaller AC field are applied in parallel to the microwave magnetic field, while temperature is scanned. This parallel geometry suppresses the typical EPR resonant response. These techniques have primarily been used in the detection and characterization of superconductors [3–5], but some research has focused on other materials [6–8] including bulk Fe_3O_4 (magnetite) [9].

Superconductors produce a characteristic peak in the MFMMS signal at the superconducting transition. Although there has been some research on nonsuperconducting materials, the response of nonsuperconducting phase transitions in the MFMMS is not well understood. Superconducting transitions in the MFMMS consistently produce a characteristic peak. However, magnetic transitions exhibit substantial variations in their MFMMS responses including a broad range of MFMMS signals. Without understanding these differing responses, it is difficult to draw conclusions from the MFMMS signal of magnetic samples.

Previous studies of the Verwey transition in Fe_3O_4 [10] have found changes in the MFMMS response across the transition [9,11]. However, since the Verwey transition is a magnetic, resistive, and structural transition, it is difficult to determine the physical origins of the features observed in the MFMMS response. In this Letter, the MFMMS, magnetic, and resistive measurements of Fe_3O_4 thin films are compared. An explanation of the physical origins of the features observed in the MFMMS is presented. This serves both as a study of the Verwey transition itself and as an analysis of the MFMMS response to magnetic transitions in general.

II. MFMMS TECHNIQUE

In a microwave cavity, the power loss density can be defined in general as

$$\frac{dP}{dV} = \frac{1}{2}(\sigma'|E_{mw}|^2 + \omega\varepsilon''|E_{mw}|^2 + \omega\mu''|H_{mw}|^2), \quad (1)$$

where μ'' is the imaginary component of the complex absolute permeability $\mu = \mu' - i\mu''$ and ε'' is the imaginary component of the complex absolute permittivity $\varepsilon = \varepsilon' - i\varepsilon''$ [12–14]. H_{mw} and E_{mw} are the microwave magnetic and electric fields, ω is the microwave frequency, and σ' is the real conductivity. In Eq. (1), the three terms on the right side correspond to the Joule loss, dielectric loss, and magnetic loss, respectively.

*Present address: National High Magnetic Field Laboratory, Los Alamos National Laboratory, Los Alamos, New Mexico 87544; corresponding author: jamespwampler@gmail.com

The MFMMS signal is defined as

$$\text{MFMMS} = \frac{dP}{dH} \tag{2}$$

which for most bulk metallic nonsuperconducting samples simplifies to the surface integral [5]

$$P = \frac{1}{2}\iint R_S |H_{mw}|^2 dA. \tag{3}$$

In Eq. (3), R_S is the surface resistance, defined as

$$R_S = \sqrt{\frac{\mu'\omega}{2\sigma'}}, \tag{4}$$

where σ' is the real component of the complex conductivity $\sigma = \sigma' - i\sigma''$ [5,15,16]. Equations (3) and (4) are true for bulk metallic samples with sufficiently low τ, the magnetic relaxation time of the material, for which $\omega\tau \ll 1$. Because $B = \mu H = \mu_0(H + M)$, it is possible to derive a proportionality between the MFMMS signal and electromagnetic properties,

$$\frac{dR_S}{dH} = \sqrt{\frac{\rho'\omega}{8\mu'}}\left(\frac{d\mu'}{dH} + \frac{\mu'}{\rho'}\frac{d\rho'}{dH}\right), \tag{5}$$

where H is the sum of the applied AC and DC magnetic fields and $\rho' = 1/\sigma'$ is the real resistivity. To reduce this to more easily measurable properties, a geometric factor a can be defined such that $aR = \rho'$ and $m/V = M$, where V is the sample volume. Substituting these into Eq. (5),

$$\frac{dR_S}{dH} = \sqrt{\frac{a\omega\mu_0}{8V}}\left(\sqrt{\frac{R}{V + \frac{m}{H}}}\frac{H\frac{dm}{dH} - m}{H^2} + \sqrt{\frac{V + \frac{m}{H}}{R}}\frac{dR}{dH}\right) \tag{6}$$

can be derived. Notably, the right side of Eq. (6) is comprised only of known constants, R, dR/dH, M, and dM/dH. The latter four quantities can be estimated with isothermal magnetic hysteresis loops and magnetoresistance measurements from which the MFMMS signal can be modeled. Note that when dR/dH and dM/dH are measured in DC field, both the reversible and irreversible changes will be measured, whereas AC field measurements such as MFMMS are sensitive only to the reversible changes. For samples with hysteretic behavior, this will reduce the accuracy of this model.

For nonmetallic samples, including Fe_3O_4 [17], there will be additional contributions to the absorbed microwave power from the permittivity and the imaginary components of the permeability and conductivity. A more complete model will be examined in Eqs. (7)–(10). However, when compared to Eqs. (3)–(6), the more complete model is substantially more difficult to measure. For this reason, this study attempts to learn as much as possible about MFMMS data in terms of measurements that can be quickly taken in commonly available techniques. As such, this Letter will compare the calculated, real, thickness-independent component of the MFMMS signal [Eq. (6)] to MFMMS measurements of Fe_3O_4 thin films and determine what conclusions can be reached from this comparison.

It is customary to assume that E and H decay with a characteristic length equal to the penetration depth, which can be expressed in general as [18,19]

$$\delta = \frac{1}{\sqrt{2}\omega}\{\varepsilon''\mu'' - \varepsilon'\mu' + [(\varepsilon'\mu')^2 + (\varepsilon''\mu'')^2 + (\varepsilon'\mu'')^2 + (\varepsilon''\mu')^2]^{1/2}\}^{-1/2}, \tag{7}$$

where ω indicates the microwave frequency in free space. Given this, integrating over the sample's thickness gives that the power absorbed in the film is

$$\frac{dP}{dA} = \frac{dP}{dV}(1 - e^{-2d/\delta})\left(\frac{\delta}{2}\right), \tag{8}$$

which can be expressed in terms of the power absorbed as

$$P = \frac{1}{2}\iint \frac{|E_{mw}|^2\delta}{2}\left(\sigma' + \omega\varepsilon'' + \frac{\omega\mu''|H_{mw}|^2}{|E_{mw}|^2}\right) \times (1 - e^{-2d/\delta})dA. \tag{9}$$

In the limit that $|H_{mw}| \gg |E_{mw}|$, which is true by the geometry of the cavity [5], we can simplify Eq. (9) to

$$P = \frac{1}{2}\iint \frac{\delta\omega\mu''}{2}|H_{mw}|^2\,(1 - e^{-2d/\delta})dA. \tag{10}$$

Note that this is simply a more general version of Eqs. (3) and (4), although in order to compare this equation to the MFMMS signal, it is necessary to take the derivative of absorbed microwave power, P, by the magnetic field, H.

III. EXPERIMENTAL RESULTS

High-quality thin-film samples of Fe_3O_4 ranging from 50 to 100 nm in thickness were grown on MgO(001) substrates by reactive sputtering in an Ar/O_2 environment. MgO was chosen as the substrate because it is a good insulator that does not produce any background microwave absorption signal. The oxygen partial pressure during deposition was 0.1 mTorr while the total deposition pressure was 2 mTorr. MgO substrates were heated at 500 °C for 45 min prior to the deposition to ensure a good film-substrate interface. Subsequent x-ray diffraction measurements at 800 eV of the Fe_3O_4(001) peak [Fig. 1(a)] were used to characterize the structural quality.

The films showed the characteristic metal-insulator transition at 116 K as shown by the resistance measurement in Fig. 1(b) (yellow curve). A change in magnetic moment was also observed near the phase transition in Fig. 1(b) (red curve) indicating the reorientation of the Fe magnetic moment. Both the resistance and magnetization data are in agreement with literature [20,21].

The electronic Verwey transition is also accompanied by a structural transition from a high-temperature cubic phase to a low-temperature monoclinic phase. The monoclinic phase can be characterized by examining the (0 0 1) Bragg peak [Fig. 1(a)] that is forbidden in the cubic phase. Due to electronic ordering, the $(0\,0\,\frac{1}{2})$ superlattice peak is only present in the monoclinic phase and can be accessed by performing x-ray scattering measurements at the Fe L-edge and O K-edge resonant energies [22–24]. By monitoring the intensity of the superlattice peak at these resonant energies, we indirectly

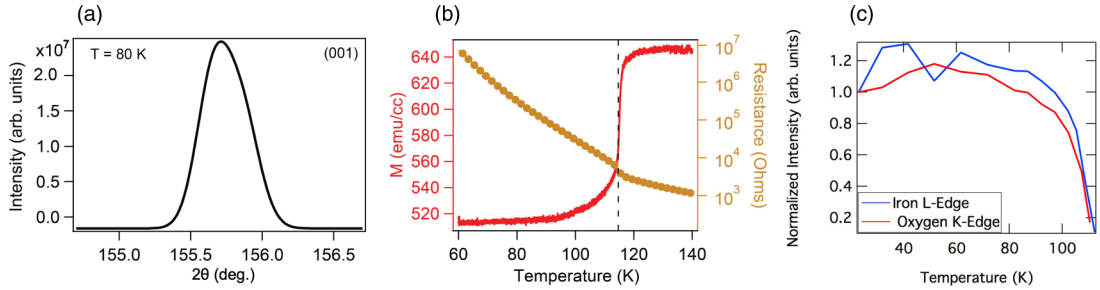

FIG. 1. Characterization of 50-nm Fe_3O_4 thin films on MgO. (a) The structural integrity of the film characterized from the (0 0 1) Bragg peak from x-ray diffraction in the monoclinic phase. (b) Magnetic and resistance measurements to pinpoint the electronic Verwey transition temperature. (c) The integrated intensity of the (0 0 $\frac{1}{2}$) superlattice peak measured at the Fe L-edge and O K-edge resonant energies, normalized to their value at 20 K. This shows the monoclinic to cubic structural transition occurring at the Verwey transition, just below 120 K.

follow the structural transition where the peak intensity disappears at about 115 K [Fig. 1(c)], which matches the resistance data shown in Fig. 1(b).

The Fe_3O_4 thin film was mounted on a quartz rod with vacuum grease and inserted into the MFMMS so that both AC and DC magnetic fields are oriented parallel to the film plane. MFMMS was measured in a fixed 15 Oe AC magnetic field, and in a 15–1600 Oe range of applied DC magnetic fields (Fig. 2). Measurements were taken by increasing the DC field between measurements. At 105 K, a steplike transition was observed in the MFMMS signal: At lower DC fields (800 Oe and below), the MFMMS signal sharply decreases as temperature increases. In contrast, at high (1100–1600 Oe) DC fields, the MFMMS signal sharply increases. At intermediate fields (between 200 and 800 Oe), a peak appears in the MFMMS signal around 105 K. This switching-step transition and peak in the MFMMS signal highly depends on the applied magnetic field and is produced by the Verwey transition. From this data alone, it is impossible to determine which electrical or magnetic attribute of the Verwey transition corresponds to each of the features observed in MFMMS. Note that 105 K is lower than one would expect for the Verwey transition and we observe an ∼10 K offset between the transition observed in the MFMMS signal and the transition observed in the magnetic and electric measurements. This 10 K offset can come from multiple sources: it can be a thermal lag between the sample and the thermometer in the MFMMS measurements,

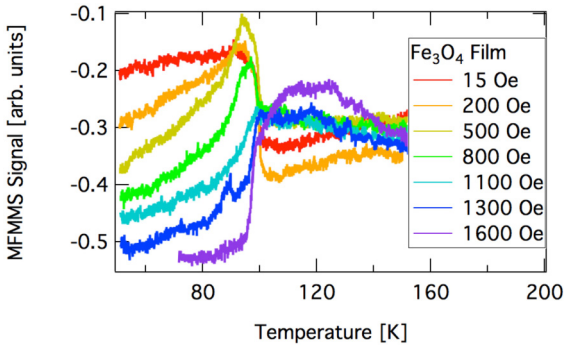

FIG. 2. MFMMS temperature sweeps of Fe_3O_4 films at a range of DC fields and 15 Oe AC field, applied in parallel to the microwave magnetic field. Temperature was swept from low temperature to high during measurements.

it can be affected by the thermal coupling between the thin film and the substrate, and it can be attributed partially to microwave heating of the magnetite particles, as previously observed [25]. In addition, previous measurements of bulk and thin-film magnetite samples have indicated that there can be sample-dependent peaks in the heat capacity across the transition in thin-film samples [26] that could affect these factors and could result in the thermal offset varying with temperature. While this thermal offset presents some uncertainty in the temperature calibration, this will not affect the conclusions reached in this study.

To investigate how the DC electric and magnetic behavior of the sample contributes to the MFMMS signal, a series of isothermal magnetic hysteresis loops and magnetoresistance measurements were taken. These measurements ranged from 90 to 145 K with the highest measurement density between 110 and 115 K, where the Verwey transition was observed in these measurements. To construct plots showing magnetic and resistive properties as a function of temperature, data points were taken from each isothermal measurement, at a given magnetic field (Supplemental Material Fig. S1) [27]. In this way, resistive and magnetic properties, as well as the magnetic field derivatives of those properties could be plotted against temperature for a range of magnetic fields (Fig. 3).

The magnetic moment in these films has a sharp step at the Verwey transition, increasing as temperature increases [Fig. 3(a)]. This is true at all fields, although it is largest at lower fields. The magnetic field derivative of the magnetic moment sharply increases as temperature increases at low fields [Fig. 3(b)]. This switches to a sharp decrease at higher fields. This indicates that the magnetic behavior is likely responsible for the switching-step behavior in the MFMMS response.

There is a sharp peak in the magnetoresistance at all fields at the Verwey transition [Fig. 3(c)]. The magnetic field derivative of the resistance also has a peak at lower applied magnetic fields [Fig. 3(d)]. It is unclear which of these is responsible for the peak in the MFMMS behavior, but the peak is clearly related to the resistive properties of the film. Combined, these figures demonstrate the behavior observed in the MFMMS response of the film: there is a step in the magnetic properties, and a peak in the resistive properties.

Fe_3O_4 exhibits a structural change across the Verwey transition [29], which raises the concern that there could be strain effects between the substrate and film which could account

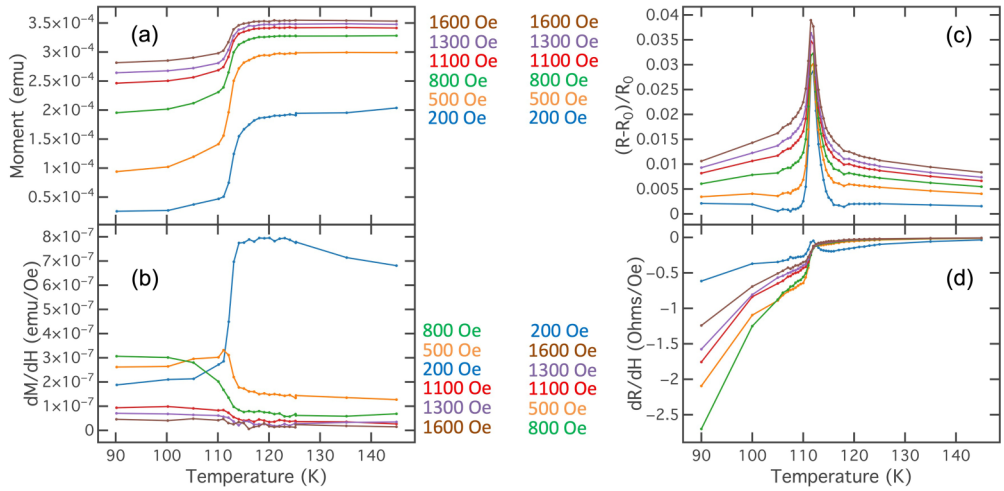

FIG. 3. Magnetic and resistive behavior of Fe_3O_4 thin films as a function of temperature. Magnetic moment (a), its derivative with magnetic field (b), magnetoresistance (c), and the magnetic field derivative of the resistance (d) are presented at a range of applied DC fields (200–1600 Oe). Data is taken from isothermal magnetic hysteresis loops and magnetoresistance measurements (Supplemental Material Fig. S1) [27]. For each subfigure, the legend indicates the ordering of data at low temperature (e.g., at low temperature, data taken with 1600 Oe magnetic field has the highest magnetic moment).

for some of the features in the MFMMS signal. However, a previous MFMMS study of bulk Fe_3O_4 at $H_{DC} = 600$ Oe exhibits similar peak and switching-step features to the 500 Oe data from this study, indicating that the features observed in this study are not a result of strain effects with the substrate (MFMMS is referred to as "MAMMAS" in that work) [9]. Furthermore, the magnetization data from Fig. 3(a) is consistent with single crystal bulk Fe_3O_4 [30]. Since the field derivative of magnetization appears to be responsible for the switching-step behavior observed in MFMMS, this also indicates that we could expect a similar feature in bulk samples. Therefore the features highlighted in this study are unlikely to be significantly affected by strain.

Using these data and Eq. (6), it is possible to calculate a model of the thickness-independent, real component of the MFMMS signal, which will be referred to from this point on as the "calculated MFMMS signal." To do this, the data in Fig. 3 was linearly interpolated, to allow for easy calculation, and then inserted into Eq. (6). This was done for the complete temperature range for each field in Fig. 3. To compare this calculated MFMMS data to the experimental MFMMS data, the calculated data was rescaled and shifted vertically (Fig. 4).

The calculated MFMMS data is particularly successful at reproducing the high-temperature behavior of the experimental data. The steplike transitions in the calculated and experimental MFMMS data are in the same direction at each field. The step switches sign between 800 and 1100 Oe in both the calculated and experimental data [Figs. 4(c) and 4(d)]. Furthermore, the shape of the high-temperature behavior is similar in the calculated and experimental data. However, there are some significant differences, most noticeably in the low-temperature behavior. In addition, while there is a peak

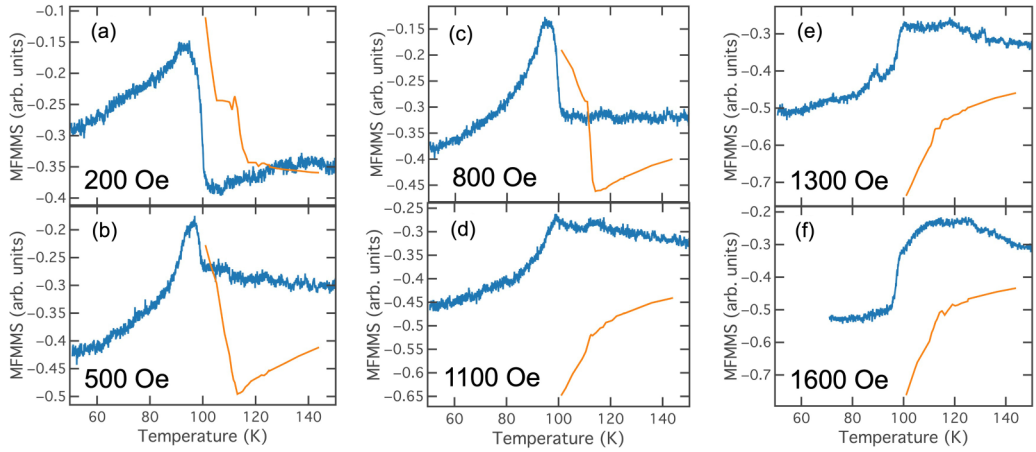

FIG. 4. MFMMS measurements of Fe_3O_4 thin films (blue; noisier data) and data calculated from magnetic and resistive data (orange; smoother data). Measurements are presented with a range of DC magnetic fields (a)–(f). To facilitate this comparison, calculated data is vertically scaled and offset. Note that the difference in the transition temperatures observed in experimental and calculated data is a result of the MFMMS flow cryostat (see above).

observed in the calculated MFMMS data at 200 Oe [Fig. 4(a)], it is much smaller than that observed in the experimental data and does not persist to higher fields. The peak behavior observed in the magnetoresistance data, which is apparent at all fields, is not exhibited by the calculated data.

While this limited model cannot be expected to capture the full behavior of nonmetallic thin-film samples in MFMMS, it is still possible to draw useful conclusions from comparing magnetic and magnetoresistive measurements (Fig. 3) and the calculated MFMMS data (Fig. 4, orange data) to the measured data. From these, we note that the step is a product of the DC magnetic behavior, while the peak observed in the MFMMS is likely a result of the magnetoresistive properties of the film. These results also suggest that least-squares fitting of the parameters from Eq. (10) that are not measured here might allow for a deeper understanding of the MFMMS behavior. Although a full investigation of this is beyond the scope of this Letter, see Supplemental Material Fig. S3 [27] for a simple fitting investigation demonstrating the potential of this strategy.

These conclusions are important because understanding the MFMMS signal of some nonsuperconducting transitions has previously been an intractable problem. This technique can thus quickly facilitate the analysis of nonsuperconducting transitions in the MFMMS. This is crucial, because MFMMS is best used as a first screening technique, quickly taking highly sensitive measurements of both majority and minority phases of samples. While it fulfills that role for superconducting samples, it has been difficult until now to properly study other electromagnetic phase transitions in this system. Given that the technique is already more sensitive than competing techniques, this increase in the analysis capabilities of the MFMMS will open new avenues of analysis of magnetic and multiphase samples.

We would like to thank Claudio Mazzoli, Wen Hu, Andi Barbour, and Stuart Wilkins for their technical support in the structural transition measurements. The collaborative aspects of this research were supported by the National Science Foundation under Grants No. DMR-1805585 and No. DMR-2007316. The superconducting aspects were funded by the National Science Foundation EAGER program under Grant No. DMR-2132389. This research used resources from the 23-ID-1 Coherent Soft X-Ray Scattering (CSX) beamline of the National Synchrotron Light Source II, a U.S. Department of Energy (DOE) Office of Science User Facility operated for the DOE Office of Science by Brookhaven National Laboratory under Contract No. DE-SC0012704. X-ray and synchrotron measurements were supported by DOE-BES under Award No. DE-SC0001805. J.G.R. acknowledges support from Vicerrectoria de Investigaciones and Facultad de Ciencias from Universidad de los Andes while in STAI at UC San Diego.

[1] K. Khachaturyan, E. R. Weber, P. Tejedor, A. M. Stacy, and A. M. Portis, Microwave observation of magnetic field penetration of high-T_c superconducting oxides, Phys. Rev. B **36**, 8309 (1987).

[2] A. M. Portis, K. W. Blazey, K. A. Müller, and J. G. Bednorz, Microwave magneto-surface impedance of high-T_c superconductors, Europhys. Lett. **5**, 467 (1988).

[3] D. Lederman, D. C. Vier, D. Mendoza, J. Santamaría, S. Schultz, and I. K. Schuller, Detection of new superconductors using phase-spread alloy films, Appl. Phys. Lett. **66**, 3677 (1995).

[4] G. K. Padam, S. N. Ekbote, M. R. Tripathy, G. P Srivastava, and B. K. Das, Non-resonant microwave absorption studies in $Bi_{1.6}Pb_{0.4}Sr_2Ca_2Cu_3O_{10+x}$, Phys. C (Amsterdam, Neth.) **315**, 45 (1999).

[5] J. G. Ramírez, A. C. Basaran, J. de la Venta, J. Pereiro, and I. K. Schuller, Magnetic field modulated microwave spectroscopy across phase transitions and the search for new superconductors, Rep. Prog. Phys. **77**, 093902 (2014).

[6] R. K. Kremer, B. Kanellakopulos, P. Bele, H. Brunner, and F. A. Neugebauer, Weak ferromagnetism and magnetically modulated microwave absorption at low magnetic fields in 1,3,5-triphenyl-6-oxoverdazyl, Chem. Phys. Lett. **230**, 255 (1991).

[7] G. Alvarez, R. Font, J. Portelles, R. Zamorano, and R. Valenzuela, Microwave power absorption as a function of temperature and magnetic field in the ferroelectromagnet $Pb(Fe_{1/2}Nb_{1/2})O_3$, J. Phys. Chem. Solids **68**, 1436 (2007).

[8] T. Saerbeck, J. Pereiro, J. Wampler, J. Stanley, J. Wingert, O. G. Shpyrko, and I. K. Schuller, Ferromagnetism in partially oxidized CuCl, J. Magn. Magn. Mater. **346**, 161 (2013).

[9] M. P. Gutiérrez, G. Alvarez, H. Montiel, R. Zamorano, and R. Valenzuela, Study of the Verwey transition in magnetite by low field and magnetically modulated non-resonant microwave absorption, J. Magn. Magn. Mater. **316**, e738 (2007).

[10] F. Walz, The Verwey transition—A topical review, J. Phys.: Condens. Matter **14**, R285 (2002).

[11] S. Guénon, J. G. Ramírez, A. C. Basaran, J. Wampler, M. Thiemens, S. Taylor, and I. K. Schuller, Search for superconductivity in micrometeorites, Sci. Rep. **4**, 7333 (2014).

[12] M. Hotta, M. Hayashi, A. Nishikata, and K. Nagata, Complex permittivity and permeability of SiO_2 and Fe_3O_4 powders in microwave frequency range between 0.2 and 13.5 GHz, ISIJ Int. **49**, 1443 (2009).

[13] J. Sun, W. Wang, and Q. Yue, Review on microwave-matter interaction fundamentals and efficient microwave-associated heating strategies, Materials (Basel). **9**, 231 (2016).

[14] Z. Peng, J.-Y. Hwang, and M. Andriese, Magnetic loss in microwave heating, Appl. Phys. Express **5**, 5 (2012).

[15] F. J. Owens and C. P. J. Poole, *Electromagnetic Absorption in the Copper Oxide Superconductors* (Kluwer Academic, New York, 1999), pp. 143–144.

[16] C. V. Topping and S. J. Blundell, A.C. susceptibility as a probe of low-frequency magnetic dynamics, J. Phys.: Condens. Matter **31**, 013001 (2019).

[17] S. Ni, X. Sun, X. Wang, G. Zhou, F. Yang, J. Wang, and D. He, Low temperature synthesis of Fe_3O_4 micro-spheres and its microwave absorption properties, Mater. Chem. Phys. **124**, 353 (2010).

[18] Z. Peng, J. Y. Hwang, J. Mouris, R. Hutcheon, and X. Huang, Microwave penetration depth in materials with non-zero magnetic susceptibility, ISIJ Int. **50**, 1590 (2010).

[19] Z. Peng, J. Y. Hwang, C. L. Park, B. G. Kim, and G. Onyedika, Numerical analysis of heat transfer characteristics in microwave heating of magnetic dielectrics, Metall. Mater. Trans. A **43**, 1070 (2012).

[20] D. T. Margulies, F. T. Parker, F. E. Spada, R. S. Goldman, J. Li, R. Sinclair, and A. E. Berkowitz, Anomalous moment and anisotropy behavior in Fe_3O_4 films, Phys. Rev. B **53**, 9175 (1996).

[21] G. Q. Gong, A. Gupta, G. Xiao, W. Qian, and V. P. Dravid, Magnetoresistance and magnetic properties of epitaxial magnetite thin films, Phys. Rev. B **56**, 5096 (1997).

[22] S. B. Wilkins, S. Di Matteo, T. A. W. Beale, Y. Joly, C. Mazzoli, P. D. Hatton, P. Bencok, F. Yakhou, and V. A. M. Brabers, Critical reexamination of resonant soft x-ray Bragg forbidden reflections in magnetite, Phys. Rev. B **79**, 201102(R) (2009).

[23] J. Schlappa, C. Schussler-Langeheine, C. F. Chang, H. Ott, A. Tanaka, Z. Hu, M. W. Haverkort, E. Schierle, E. Weschke, G. Kaindl, and L. H. Tjeng, Direct Observation of T2g Orbital Ordering in Magnetite, Phys. Rev. Lett. **100**, 026406 (2008).

[24] R. Kukreja, N. Hua, J. Ruby, A. Barbour, W. Hu, C. Mazzoli, S. Wilkins, E. E. Fullerton, and O. G. Shpyrko, Orbital Domain Dynamics in Magnetite Below the Verwey Transition, Phys. Rev. Lett. **121**, 177601 (2018).

[25] F. Sakran, A. Copty, M. Golosovsky, D. Davidov, and P. Monod, Scanning ferromagnetic resonance microscopy and resonant heating of magnetite nanoparticles: Demonstration of thermally detected magnetic resonance, Appl. Phys. Lett. **84**, 4499 (2004).

[26] C. L. Snow, Q. Shi, J. Boerio-Goates, and B. F. Woodfield, Heat capacity studies of nanocrystalline magnetite (Fe_3O_4), J. Phys. Chem. C **114**, 21100 (2010).

[27] See Supplemental Material at http://link.aps.org/supplemental/10.1103/PhysRevB.106.L060402 for a detailed description of magnetoresistance and magnetization measurements and a short discussion on using least-squares fitting to supplement these measurements, which also includes Ref. [28].

[28] A. Savitzky and M. J. E. Golay, Smoothing and differentiation of data by simplified least squares procedures, Anal. Chem. **36**, 1627 (1964).

[29] J. Blasco, J. García, and G. Subías, Structural transformation in magnetite below the Verwey transition, Phys. Rev. B **83**, 104105 (2011).

[30] R. Prozorov, T. Prozorov, S. K. Mallapragada, B. Narasimhan, T. J. Williams, and D. A. Bazylinski, Magnetic irreversibility and the Verwey transition in nanocrystalline bacterial magnetite, Phys. Rev. B **76**, 054406 (2007).